Shifted excitation Raman difference spectroscopy with charge-shifting charge-coupled device (CCD) lock-in detection

Kay Sowoidnich, Michael Towrie, Martin Maiwald,
Bernd Sumpf, and Pavel Matousek

Published version information

Citation: K Sowoidnich et al. "Shifted excitation Raman difference spectroscopy with charge-shifting charge-coupled device (CCD) lock-in detection." Applied Spectroscopy, vol. 73, no. 11 (2019): 1265–1276.

DOI: 10.1177/0003702819859352

Shifted Excitation Raman Difference Spectroscopy with Charge-Shifting CCD Lock-In Detection

Kay Sowoidnich[1,2], Michael Towrie[1], Martin Maiwald[2], Bernd Sumpf[2], Pavel Matousek[*,1]

1) Central Laser Facility, Research Complex at Harwell, STFC Rutherford Appleton Laboratory, UKRI, Harwell Campus, OX11 0QX, UK

2) Ferdinand-Braun-Institut, Leibniz-Institut für Höchstfrequenztechnik, Gustav-Kirchhoff-Str. 4, 12489 Berlin, Germany

* Corresponding author: E-mail: pavel.matousek@stfc.ac.uk

Abstract

Shifted excitation Raman difference spectroscopy (SERDS) can provide effective chemically specific information on fluorescent samples. However, the restricted ability for fast detection (usually < 10 Hz) of spectra excited at two shifted laser wavelengths can limit its effectiveness when rapidly varying emission backgrounds are present. This paper presents a novel charge-shifting lock-in approach permitting fast SERDS operation (exemplarily demonstrated at 1000 Hz) using a specialized dual-wavelength diode laser (emitting at 829.40 nm and 828.85 nm) and a custom built CCD enabling charge retention and shifting back and forth on the CCD chip. For six selected mineral samples (moved irregularly during spectral acquisition) results demonstrate superior reproducibility of the fast charge-shifting read-out over the conventional read-out (operated at 5.4 Hz). Partial least squares-discriminant analysis revealed improved classification performance of charge shifting (4 latent variables, sensitivity: 99 %, specificity: 94 %) versus conventional read-out (6 latent variables, sensitivity: 90 %, specificity: 92 %). The charge-shifting concept was also successfully translated to sub-surface analysis using spatially offset Raman spectroscopy (SORS). Charge-shifting SERDS-SORS spectra recorded from a polytetrafluoroethylene layer concealed behind a 0.25 mm thick opaque heterogeneous layer matched reference spectra much more closely and exhibited a signal-to-background-noise-ratio two times higher than that achieved with conventional CCD read-out SERDS-SORS. The novel approach overcomes fundamental limitations of conventional CCDs. In conjunction with the inherent capability of the charge-shifting lock-in technique to suppress rapidly varying ambient light interference demonstrated by us earlier it is expected to be particularly beneficial with heterogeneous fluorescent samples in field applications.

Keywords: Raman spectroscopy, optical lock-in detection, shifted excitation Raman difference spectroscopy, spatially offset Raman spectroscopy, sample heterogeneity

Short title: SERDS with Charge-Shifting CCD Lock-In Detection

1. Introduction

Raman spectroscopy is a powerful tool in a variety of applications due to its ability to provide chemically specific information on the sample under investigation. One of the major issues of the technique is however its susceptibility to fluorescence interference which can easily overwhelm the weak Raman signals by many orders of magnitude. Due to the potential severity of the fluorescence problem a wide range of fluorescence rejection techniques has been developed which can be coarsely divided into computational and experimental approaches. [1] The mathematical methods [2, 3] are usually relatively easy to implement and do not require setup modifications but have limited capability in fluorescence removal. Temporal gating techniques [4, 5] can be very powerful as they exploit the fact that Raman scattering and fluorescence occur on different time scales. The application of short-pulsed lasers (picoseconds or shorter) and gated detection can efficiently separate the Raman signal (generated practically instantaneously after laser excitation) from the unwanted fluorescence contribution (generated often in the range of nanoseconds after laser excitation). Despite its remarkable performance, also stemming from the fact that a large part of fluorescence is typically prevented from being detected and therefore eliminating contamination of Raman signal by its photon shot noise, the gating approach is not widely used due to the requirement for more complex and more expensive instrumentation [6] which also makes it less practical for portable systems.

Another promising method for mitigation of fluorescence effects employs two slightly different laser excitation wavelengths. Provided the spectral difference is small enough the broadband fluorescence will remain essentially unchanged while the Raman signals will experience a spectral shift when switching from one laser wavelength to another. The subtraction of the two spectra from each other effectively reduces fluorescence and associated background distortions born in the detection system yielding out a Raman spectrum in a 'differential' form, with diminished fluorescence background (although it should be noted the photon shot noise associated with the subtracted fluorescence background is carried through into the Raman spectrum in full). From this the original Raman spectrum can be readily reconstructed mathematically. [7] In its basic implementation, this concept is known as shifted excitation Raman difference spectroscopy (SERDS) [8, 9] but similar techniques applying a multitude of neighboring excitation wavelengths [10, 11] have been demonstrated as well. The advantage of SERDS is that the only significant modification compared to conventional Raman spectroscopic set-ups is the implementation of a light source with two different emission wavelengths. Using compact microsystem diode lasers for excitation has therefore enabled the realization of portable SERDS instruments [12] as well as devices using more than two excitation wavelengths. [13, 14]

The increasing availability of suitable laser sources for SERDS in the relevant spectral regions from the visible to the near infrared has boosted research in numerous fields. For example regarding food quality monitoring the benefits of SERDS have been shown for meat inspection, [15] precision agriculture [16] and the analysis of alcoholic beverages. [17, 18] In the

biomedical area studies in the field of cancer detection [19, 20] and research to optimize experimental parameters and data processing for diagnostic purposes [21, 22] have been reported. To enhance the weak Raman signals, SERDS has been combined also with resonance Raman spectroscopy for the quantification of carotenoids in human skin, [23] the detection of food colorants at low concentration [24] and structural studies on photosynthetic proteins. [25] SERDS in combination with surface-enhanced Raman spectroscopy (SERS) shows large potential in environmental quality control for trace detection of water pollutants [26, 27]as well as for biomedical sensing applications. [28] Other examples of SERDS usage areas include the analysis of extraterrestrial particles from an asteroid, [29] monitoring of algae in a bioreactor [30] and investigations of art pigments. [31]

Despite the wide range of applications one major issue related to dealing with fast changing or unstable fluorescence backgrounds caused, for example, by sample heterogeneity, as commonly present in biological and natural specimens, and movement of sample or Raman instrument is still present. Another example of fluorescence background variation is the analysis of dynamically evolving systems (e.g. undergoing a chemical reaction or physical change, for example crystallization) or the study of photosensitive samples where photo-degradation is present. Such fluorescence background variations can only be captured effectively with a quasi-simultaneous detection of SERDS spectra at both excitation wavelengths on a time scale substantially faster than that for the corresponding background changes. Regarding the excitation light sources this is not a problem as rapid modulation between the two SERDS wavelengths has successfully been demonstrated, for example up to 1000 Hz using both distributed Bragg reflector Y-branch [32] and external cavity diode laser concepts. [33] Selected SERDS studies have also shown that short integration times down to 200 ms [34] or even 50 ms [18] are feasible. Nevertheless, read-out and analog-to-digital conversion steps impose a fundamental physical limit to the lowest achievable integration times, that is, for instance, 50 ms exposure time is followed by several tens of milliseconds of read-out and digitization steps before the next exposure can start. Additionally, a large number of multiple CCD read-outs also leads to the accumulation of CCD read-out noise which can also be an undesirable consequence of such approaches. For these reasons, the operation speed of conventional CCD based low noise detectors is limited in practice to less than 10 Hz restricting the ability of the SERDS concept to deal with the fast evolving fluorescence backgrounds described earlier, which leave unremoved background distortions in the acquired SERDS spectra.

To overcome this issue and ultimately enable rapid SERDS detection at kilohertz repetition rates we exploit the benefits of a CCD charge-shifting technique. [35, 36] The concept was demonstrated first in Raman spectroscopy by Heming *et al*. with a fast rotating sample cell to investigate differences between light-activated and dark-adapted membrane proteins [37] and later by our group for the efficient rejection of varying ambient light from Raman spectra. [38] The key benefit of the charge-shifting approach is that the usual read-out and digitization steps are not performed after each exposure but only once at the end of the

entire measurement, e.g. after many thousands of cycles. It is important to note that physically the same pixels on the CCD chip are illuminated with both the excitation wavelengths while only the corresponding charges are shifted in the electronic register. A penalty in this mode is a need for utilization of a part of the CCD area for storing the shifted charge which is not illuminated at each step by any signal – between one half and two thirds of the CCD area is typically required for this depending on the number of shifted rows.

In this paper, we demonstrate SERDS with charge-shifting CCD lock-in detection, experimentally realized with a custom made charge-shifting CCD detector in combination with a specialized microsystem diode laser for SERDS. The system was first characterized on heterogeneous and fluorescent mineral specimens. A number of natural rocks were used in this study aiming at obtaining representative average spectra of different rock types suitable for classification purposes. Another challenging measurement scenario with usually an order of magnitude lower signal intensities than those present in conventional Raman analysis is the sub-surface investigation of turbid media applying spatially offset Raman spectroscopy (SORS).[39, 40] To assess the capabilities of the charge-shifting SERDS technique under such demanding conditions, the concept was extended by combining it with SORS to enable sub-surface analysis of turbid stratified samples, exemplarily demonstrated on a layer of polytetrafluoroethylene (PTFE) obscured by an opaque heterogeneous layer. In both the cases, charge-shifting data obtained at 1000 Hz were compared with a fast conventional read-out carried out at 5.4 Hz (which is the maximum read-out frequency achievable by the CCD under the selected operation conditions) to evaluate the performance of this new approach.

2. Materials and Methods

2.1. Charge-shifting SERDS setup

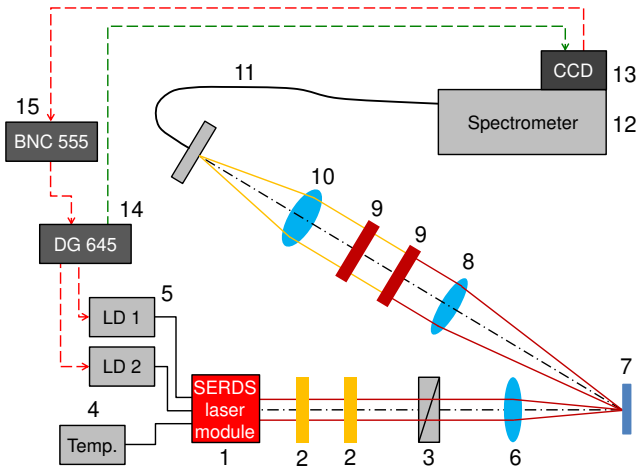

Figure 1: Schematics of charge-shifting SERDS setup with dual-wavelength SERDS laser module emitting light at around 830 nm (1), band pass filter (2), quarter waveplate (3), laser temperature controller (4), laser drivers (5), lenses (6, 8, 10),

specimen (7), Raman edge filter (9), optical fiber (11), spectrometer (12), charge-shifting CCD (13), SRS DG645 digital delay generator (14) and BNC model 555 digital delay generator (15), the dashed red and green lines with arrows indicate electrical connections for timing synchronization.

Figure 1 depicts a scheme of the charge-shifting SERDS setup utilizing a purpose designed SERDS laser module [41] from Ferdinand-Braun-Institut as the excitation light source. The device (1) contains two separate laser cavities emitting at λ_1 = 829.40 nm and λ_2 = 828.85 nm to realize a spectral shift for SERDS of 8 cm^{-1}. The collimated and linearly polarized laser light passes through two bandpass filters (LL01-830-25, Semrock, Inc.) (2) and is subsequently converted into circularly polarized light by means of a quarter waveplate (WPQ05M-830, Thorlabs) (3). To achieve a common output aperture in combination with high optical output powers for the two excitation wavelengths, both the laser beams were combined within the laser module using a polarization beam combiner cube. Consequently, at the common output aperture the laser beams originating from both the laser cavities have polarization states perpendicular to each other. The quarter waveplate was introduced to achieve left and right circularly polarized laser light thus minimizing linear polarization induced effects in the sample. A temperature controller (5240 TECSource, Arroyo Instruments) (4) was used to set the temperature of the laser module to 25 °C while the injection currents of both laser cavities were controlled independently by means of two laser drivers (4220-DR LaserSource, Arroyo Instruments) (5). Using a lens with a focal length of 100 mm and a diameter of 25.4 mm (LBF254-100-B, Thorlabs) (6) the excitation laser radiation was focused onto the sample (7).

In the collection arm the backscattered radiation was collected by an achromatic lens with a focal length of 100 mm and a diameter of 25.4 mm (AC254-100-B, Thorlabs) (8) and passed through two Raman edge filters (LP02-830RU-25, Semrock, Inc.) (9) to reject elastically scattered light. The transmitted Stokes shifted Raman components were imaged by an achromatic lens with a focal length of 60 mm and a diameter of 25.4 mm (AC254-060-B, Thorlabs) (10) into a round-to-linear fiber bundle (BFL200LS02, Thorlabs, Inc.) (11) which then transferred the detected light into a spectrometer (Holospec 1.8i, Kaiser Optical Systems, Inc.) (12) with a custom made charge-shifting CCD (DU420A-BR-DD-9UW, Andor Technology, S/N CCD-19689) (13) mounted on its output. The CCD was controlled by a PC running customized Andor Solis software (version 4.28.30052.0, Andor Technology) and it was thermo-electrically cooled down to -70 °C. The back and forth charge-shifting mode of operation was controlled by the Solis software which had the charge-shifting feature built in to our requirements. With respect to SORS measurements and also to prevent primary reflections from the excitation laser light off the sample surface from entering the collection path, the Raman collection arm was separated from the laser excitation arm with an angle of ca. 30° between them. Both the excitation and Raman collection arms were shielded from ambient light using a black aluminum foil cover (BKF12, Thorlabs, Inc.). Recently, we have successfully demonstrated the efficient ambient light rejection capabilities of the charge-

shifting approach. [38] However, to separate ambient light contributions from the effects caused by sample heterogeneity and variations in laser-induced fluorescence, in the present study the laboratory room light was switched off during the measurements.

To synchronize the laser emission with the charge-shifting CCD read-out one of the output ports of a digital delay generator (DG645, Stanford Research Systems) (14) was connected to the external trigger input of the CCD (13) while two other output ports were connected to the modulation inputs of the two laser drivers (5). The shutter output of the CCD was connected to the input of a second digital delay generator (Model 555, Berkeley Nucleonics Corporation) (15). The output of the Model 555 delay generator was connected to the *Inhibit* input of the DG645 delay generator to enable alternate laser emission on both excitation wavelengths only during the charge-shifting procedure but not during the final CCD read-out and digitization phase to avoid spectral mixing.

To assess the potential of the charge-shifting technique in combination with SERDS and SORS the setup shown in Figure 1 was modified to introduce a spatial offset in the excitation beam in relation to the detection beam. For that purpose, a set of two round wedge prisms (PS814-B, Thorlabs) was inserted between the focusing lens (6) and the sample (7) to realize a SORS point offset, exemplarily set to ca. 4 mm. The zero offset was realized by physically removing the pair of wedge prisms from the beam path.

2.2. Charge-shifting method

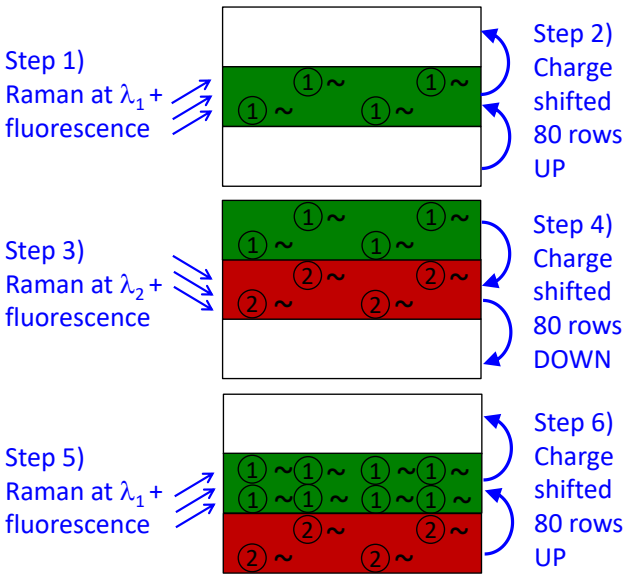

Figure 2: Illustration of the charge-shifting SERDS principle: Accumulation of charges in active area caused by Raman scattered light excited at first laser wavelength and fluorescence contributions (step 1) followed by shifting of these charges to a non-illuminated (top) storage area (step 2), Accumulation of charges due to Raman scattered light excited at second laser wavelength and fluorescence contributions in active area (step 3) and subsequent shift of these charges down to a second (bottom) non-illuminated storage area (step 4), Repetition of cycle one by accumulating more charges

caused by Raman scattered light excited at first laser wavelength and fluorescence contributions in active area (step 5) followed by shifting of these charges to the top storage area (step 6). The symbols denote charges on CCD chip created by illumination with Raman light excited at first (1) and second (2) laser wavelength as well as fluorescence interference (~).

In the charge-shifting CCD operation an external 1000 Hz trigger signal starts the first cycle in which all charges of the electronic register are shifted down by 80 rows and then a specific area on the CCD chip (usually located around the center vertically) receives Raman scattered light and fluorescence light from the sample excited at the *first* excitation wavelength and the generated charges are accumulated in charge zone 1 of the electronic register (Figure 2, step 1). After 1 ms the next trigger signal starts the second cycle with all charges of the electronic register being shifted up by 80 rows resulting in the charge zone 1 being moved to a non-illuminated CCD area (Figure 2, step 2). Subsequently, physically the same pixels on the CCD chip are illuminated by Raman scattered light and fluorescence light from the sample excited at the *second* excitation wavelength (Figure 2, step 3) but the corresponding charges are now accumulated in a different charge zone of the detector (called charge zone 2 hereafter). The next trigger signal is then starting cycle three which is identical to the first cycle, i.e. shifting all the charges in the electronic register downwards by 80 rows (Figure 2, step 4) and illuminating the CCD by Raman scattered light and fluorescence light from the sample excited at the *first* excitation wavelength adding more charge due to detected photons to the existing charge (Figure 2, step 5). During this cycle charge zone 2 is moved to an unilluminated range of the CCD while charge zone 1 is illuminated again. Subsequently, all the charges are shifted up by 80 rows again (Figure 2, step 6). The sequence of the alternate charge accumulations in the two distinct zones of the electronic register while illuminating the same pixels of the CCD chip is repeated 5,000 times, corresponding to a total acquisition time of 5 seconds. In the final step the accumulated charge on the CCD chip is read out (utilizing image mode with a vertical binning of 16 pixels applied) and digitized. For data analysis only the charges accumulated in two separated charge zones, namely those located at the end of the sequence in pixels 1-64 as well as in pixels 81-144, were used. As the illumination condition for charge zone 1 can be either with the first (λ_1) or with the second (λ_2) laser excitation wavelength there exist two different illumination geometries, called *a* (λ_1 in charge zone 1/ top area in final image and λ_2 in charge zone 2/ bottom area in final image) and *b* (λ_1 in charge zone 2/ bottom area in final image and λ_2 in charge zone 1/ top area in final image). Spectra were always recorded in pairs of *a* and *b* geometries resulting in a total acquisition time of 10 seconds (10,000 charge shifting cycles in total). This 'pair' acquisition approach was unlikely to be necessary in these measurements as it mainly reduces artefacts stemming from residual ambient light illuminating the CCD chip during its charge shifting phases (as the collection path is not equipped with any mechanical shutter to block such residual ambient light during charge shifting phases), which was in these experiments present only at very low level (e.g. display glow). The procedure is discussed and illustrated in detail in our previous publication. [38]

Both the laser drivers are set to an injection current of 0 mA and a square-wave modulation is applied by the DG 645 at a frequency of 500 Hz, i.e. firing a specific excitation wavelength only when the charge is in an identical position of the electronic register (top or bottom area) as it was for the previous corresponding laser pulse. To avoid laser emission during the time required to shift the charge 80 rows up and down (which would lead to signal mixing in the two areas), a pulse delay between CCD trigger signal and laser pulse output of 680 µs was applied. Limited by the time available until the subsequent pulse arrives (i.e. 1 ms), the laser pulse width was set to 319 µs. Further details of the charge-shifting CCD operation can be found in our previous publication. [38]

2.3. Conventional read-out

For comparison SERDS spectra were also recorded in conventional CCD read-out mode using sub-acquisition times of 100 ms. To match the illumination conditions used in charge-shifting mode 74 acquisitions and a laser pulse width of 43 ms (pulse delay: 29 ms) were used. To mimic the read-out conditions of the charge-shifting mode, spectra were acquired in multi-track mode using 4 tracks containing 16 vertical pixels each, i.e. pixels 81-144. The CCD was externally triggered at a frequency of 5.4 Hz by the DG645 delay generator to record a kinetic series with adjacent spectra corresponding to Raman spectra of the sample excited at the two distinct laser wavelengths.

2.4. Sample material

Six samples consisting of different minerals (rocks) showing a recoverable Raman signal from the fluorescence interference using SERDS (basalt, diorite, granite, granulite, pegmatite and quartzite) obtained from Fisher Scientific UK Ltd (Pangea™ Igneous Rock Collection and Pangea™ Metamorphic Rock Collection) were used in the SERDS experiments. Individual rocks were held in the hand of the operator and moved at moderate speed in an irregular pattern during spectral acquisition to mimic a sample movement often present in handheld Raman measurements. To remain in the excitation and detection focal plane the flat side of the specimens was moved perpendicular to the excitation laser beam using an aperture in the sample stage as mechanical guidance. By adjusting the voltages applied to the modulation inputs of both laser drivers, average laser powers at the sample position of 50 mW for both excitation wavelengths were realized. 18-20 repeat spectra with each method (charge shifting and conventional) were recorded for each specimen. For technical reasons, for granite only 19 pairs of *a* and *b* spectra were recorded and for granulite only 18 pairs of *a* and *b* spectra were recorded.

For the SERDS-SORS investigations the sample material consisted of a block of 4 layers of PTFE (total thickness: 8 mm) concealed behind a 0.25 mm thick layer of glossy paper with a multi-colored printed artwork on it. The entire specimen was moved by hand in an irregular pattern as above during data acquisition to introduce background variation due to the heterogeneity of the surface layer. 10 spectra were recorded for each zero and 4 mm spatial offsets. To achieve a recordable Raman signal at both the zero and non-zero SORS offsets the average laser power at the sample was set to 150 mW by adjusting the modulation input voltages of both laser drivers. As a reference spectrum the exposed PTFE block was measured at one single spot under identical conditions in the 4 mm offset configuration.

2.5. Data analysis

For the *conventional read-out* the intensities acquired on the four individual tracks (vertical pixels 81-144) were averaged and individual spectra for both excitation wavelengths in the kinetic series were accumulated leading to two averaged spectra. To account for possible variations in the background intensity between the two spectra the spectrum recorded at λ_1 (spectrum 1) was divided by the spectrum recorded at λ_2 (spectrum 2) and the resulting quotient spectrum was fitted by a seventh order polynomial function (MATLAB R2013a). In this way, a normalization function to compensate for background variations is obtained. Spectrum 2 was then multiplied by the normalization function (to adjust/match the baseline of spectrum 2 with respect to the baseline of spectrum 1) and the result was subtracted from spectrum 1 to achieve a SERDS difference spectrum with an almost flat baseline. This procedure, rather than a simple scaled subtraction, was chosen in order to more efficiently eliminate/minimize irregular background distortions. For further data analysis, no attempts were made to integrate or otherwise reconstruct the SERDS difference spectra as this step could introduce an additional, computation-induced degree of variation to the spectral data potentially obscuring or confounding effects related to the studied read-out modality. However, reconstructed SERDS spectra were exemplarily computed for basalt and PTFE using a simple reconstruction algorithm [7] and are displayed for illustrative purposes only, i.e. all calculations presented in the manuscript were carried out using the SERDS difference spectra.

In the case of the *charge shifting spectra* initially the intensities acquired in the top area (vertical pixels 81-144) for the *a* spectra and the intensities acquired in the bottom area (vertical pixels 1-64) for the *b* spectra were added to achieve a spectrum recorded at λ_1. In a similar way, a cumulative spectrum recorded at λ_2 was calculated from the bottom area of the *a* spectra and the top area of the *b* spectra. Normalization and computation of the SERDS difference spectra was then done identical to the procedure applied for conventional read-out.

The signal intensity of the most prominent Raman band of the selected samples was calculated as peak-to-valley-distance in the SERDS difference spectra. For basalt rock the signal at 1085 cm^{-1} (CO_3^{2-} symmetric stretch [42]) was used while for the other five rocks the Raman band at 466 cm^{-1} (O-Si-O bend [43]) was utilized. In the case of the PTFE specimen the calculation was done taking into account the 732 cm^{-1} band (C–F and C–C symmetric stretch [44]). The background noise level was estimated as standard deviation of SERDS difference intensities in the ranges 850-900 cm^{-1} for all the rock samples and 500-550 cm^{-1} in the case of PTFE as these spectral regions were free of any target Raman signals. The signal-to-background-noise ratio (S/BG) was determined by dividing the signal intensity of the selected Raman band by the background noise level within the individual spectra. In contrast, the signal-to-noise ratio (S/N) was defined as the average signal intensity of the selected Raman band divided by the standard deviation of the signal intensities of all repeat spectra recorded for each specimen.

Principal component analysis (PCA) was applied to assess the variation in repeat spectra for individual rocks using OriginPro 2015 software (OriginLab Corp.). Separate PCA models were evaluated for all six investigated rock specimens using 20 SERDS difference spectra each for conventional and charge-shifting spectra, i.e. 40 spectra in total per model. As preprocessing steps all spectra were truncated to the 200-1600 cm^{-1} region, normalized to their respective maximum and mean-centered.

To assess the discrimination performance between different rock types partial least squares-discriminant analysis (PLS-DA) was performed using SOLO (version 8.6.2, Eigenvector Research, Inc.). Separate models were computed for both CCD read-out modes (conventional and charge-shifting) including 20 SERDS difference spectra from all 6 rock types, i.e. 120 spectra in total per model. The preprocessing steps were identical to those performed for PCA.

3. Results and discussion

3.1. Comparison of SERDS read-out modalities

To illustrate the ability of conventional and charge-shifting CCD read-out to deal with fast background variations in spectra, as e.g. present with sample movement during spectral acquisition, Figure 3a displays the mean and standard deviation of 20 individual SERDS difference spectra for both the read-out modalities using a basalt rock as specimen. Despite applying polynomial normalization during spectral reconstruction (see previous section for details) there remain pronounced distortions in the baseline of the SERDS difference spectra recorded in the conventional read-out at 5.4 Hz with sub-acquisition times of 100 ms. Furthermore, the variation between individual spectra is increased in the conventional read-

out mode as indicated by the larger standard deviation (gray area in Figure 3). For illustrative purposes, the reconstructed SERDS spectra of basalt obtained for the two selected read-out modalities are presented in Figure 3b. The baseline distortions present in the conventional read-out SERDS difference spectra are amplified in the reconstructed SERDS spectra and are especially evident as broad features in the spectra range between 500 cm^{-1} and 800 cm^{-1}. As an example, the Raman band around 710 cm^{-1}, which is clearly visible in the reconstructed charge-shifting SERDS spectra, is significantly distorted in the reconstructed conventional read-out SERDS spectra.

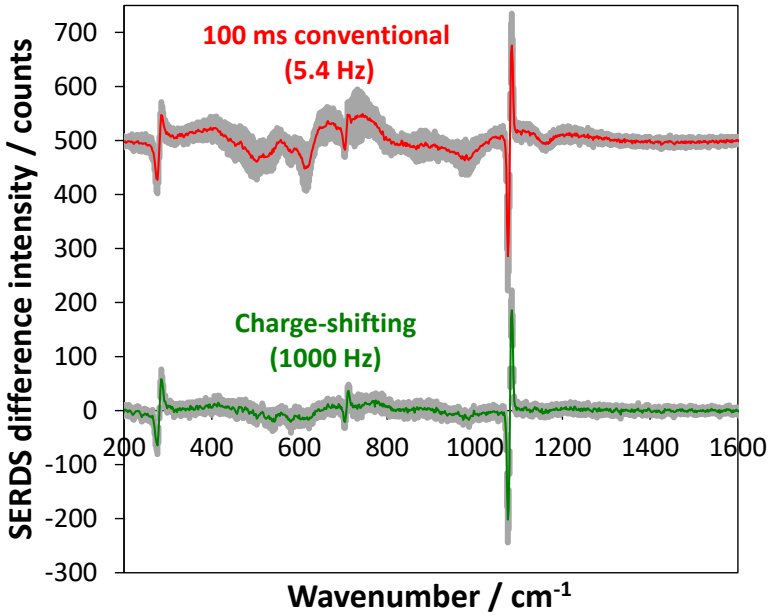

Figure 3: SERDS difference spectra of basalt rock recorded in conventional and charge-shifting CCD read-out modes. Displayed are the mean and standard deviation of 20 spectra each. The spectra are vertically offset for clarity.

For a quantitative assessment of the SERDS difference spectra, the signal-to-background-noise ratio (S/BG), the signal-to-noise ratio (S/N) and the sum of all standard deviations in the spectral range from 200 cm^{-1} up to 1600 cm^{-1} ($SD_{cumulative}$) have been calculated for all 6 rock species and are presented in Table 1. Compared to the conventional read-out spectra the S/BG as well as the S/N of the charge-shifting SERDS difference spectra is comparable with no clear trend being observable. As the CCD read-out noise is much smaller than the shot noise caused by laser-induced fluorescence, in this case, the larger number of read-outs (74 for conventional read-out but only two in charge-shifting mode) does not have a detrimental effect on spectral quality. However, the $SD_{cumulative}$, which represents the variation between repeat spectra and is also indicative of residual distortions in the spectra, is significantly reduced in the charge-shifting read-out mode by 52 % on average (min: 29 %, max: 77 %). Despite the comparable S/N and S/BG between the two read-out modes baseline distortions are clearly reduced in the charge-shifting SERDS spectra, exemplarily

shown in the case of basalt in Figure 3. This makes charge-shifting SERDS read-out advantageous not only for automatic data processing but also in such cases where weak Raman bands or band shapes are of particular interest. Consequently, the much faster modulation between the two excitation wavelengths and corresponding detection of Raman spectra at 1000 Hz provides superior reproducibility between repeat spectra recorded over slightly different areas of the heterogeneous rock specimen ultimately yielding a more representative average spectrum.

Table 1: Overview of signal-to-background-noise ratio (S/BG), signal-to-noise ratio (S/N) and cumulative standard deviation in the spectral range from 200 cm^{-1} to 1600 cm^{-1} ($SD_{cumulative}$) for the six selected rock species calculated from the SERDS difference spectra using conventional and charge-shifting read-out modes.

	Charge-shifting (1000 Hz)			**Conventional (5.4 Hz)**		
	S/BG	S/N	$SD_{cumulative}$	S/BG	S/N	$SD_{cumulative}$
Basalt	44 ± 13	5.2	6833	40 ± 10	3.3	11868
Diorite	34 ± 12	4.8	9253	37 ± 11	5.5	40368
Granite	15 ± 4	5.1	13432	14 ± 3	5.0	49344
Granulite	14 ± 3	6.1	18006	12 ± 2	6.0	35076
Pegmatite	128 ± 25	10.3	11185	133 ± 32	13.1	19067
Quartzite	54 ± 7	9.1	15774	52 ± 11	8.5	22188

Principal component analysis (PCA) is a well-established multivariate technique that allows the data variability to be determined with respect to statistical variances in the data set. Here, PCA was applied to assess the reproducibility between individual spectra recorded in conventional and charge-shifting read-out under the influence of variable measurement conditions due to sample movement during spectral acquisition. A scores plot for Basalt using principal component 1 (PC 1) and principal component 2 (PC 2) in Figure 4 shows that the data points corresponding to spectra acquired in the conventional read-out mode scatter much more than those representing the charge-shifting spectra that form a more compact cluster. In the PC 1 direction (explaining 49 % of the total variance) the conventional read-out data spreads over 0.79 length units while the charge-shifting read-out is much more confined, only extending to 0.07 length units. In direction of PC 2 (explaining 24 % of the total variance) the conventional spectra cover a range of 0.79 length units whereas the charge-shifting data is again more compact with a length of 0.25 units.

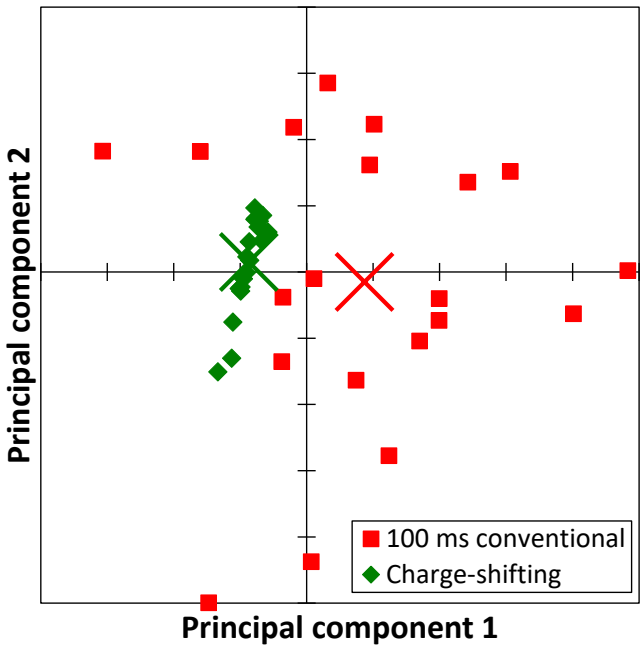

Figure 4: PCA scores plot of basalt samples recorded in conventional and charge-shifting read-out modes. Crosses indicate the mean score value for each of the two clusters which are used for vector length calculations.

To evaluate the variations present in the data sets for all the six investigated rocks the length of the individual score vectors from their respective cluster mean, as indicated by crosses in Figure 4, were calculated as Euclidean distance. The results presented in Figure 5 highlight that the mean cluster size (i.e. mean score vector length in the PC 1-PC 2-plane) as well as the variation between individual spectra (i.e. standard deviation) are clearly reduced when using the charge-shifting mode for all the investigated rock samples. On average, the mean cluster size for the conventional read-out data is larger by a factor of 4.9 compared to the charge-shifting mode while the standard deviation is 4.1-times larger. With a clear difference between the read-out modalities, the results of the multivariate analysis confirm that the fast spectral acquisition capabilities of the charge-shifting CCD read-out provide generally a superior performance with respect to conventional read-out when dealing with this type of heterogeneous specimens.

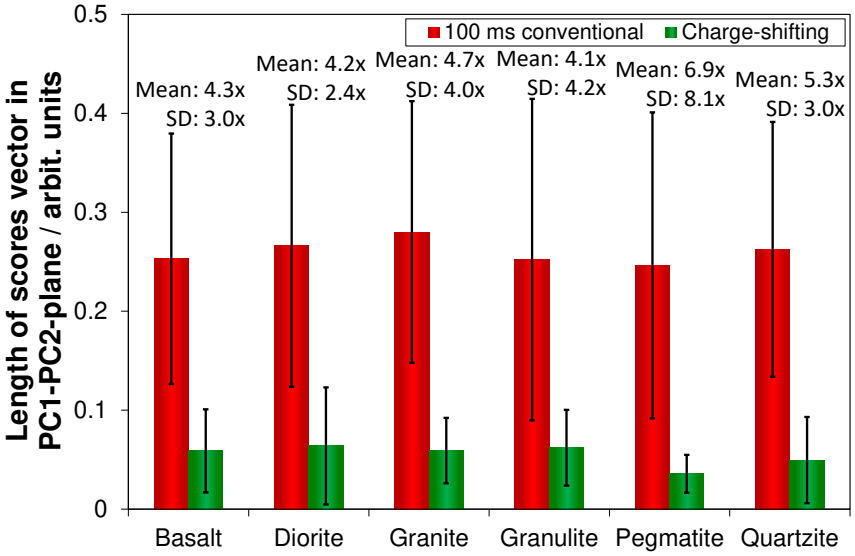

Figure 5: The mean length and standard deviation (SD) of scores vectors in PC1-PC2-plane relative to cluster center (i.e. mean score value) for data recorded in conventional (100 ms at 5.4 Hz) and charge-shifting (1000 Hz) read-out. SERDS difference spectra were normalized to maximum and mean-centered before analysis. The numbers above the bars indicate the factor by which the mean and SD of conventional read-outs are larger compared to the charge-shifting read-out.

3.2. SERDS discrimination capability between rock species

Based on the outcomes of the previous section an attempt was made to use the spectra acquired in the two distinct read-out modes for classification of the six different rock types. Separate models for conventional and charge-shifting CCD read-out were built using partial least squares-discriminant analysis (PLS-DA). The results for sensitivity and specificity using leave-one-out cross-validation are presented in Table 2. The first difference to note is that the SOLO software selected different optimal numbers of latent variables (LVs) for models built from the two read-out modalities. While four LVs were sufficient for the model derived from the charge-shifting data set, six LVs were considered necessary to describe the model based on the data set from the conventional read-out. Even with a lower number of latent variables the data set derived from the charge-shifting spectra exceeds, or at least matches, the sensitivity and specificity values achieved for the data based on the conventional read-out spectra for all the six investigated rock types. The average sensitivities and specificities for the charge-shifting data compared to the conventional data are higher by 9 % and 2 %, respectively. These results demonstrate that the improved reproducibility for individual rocks achievable by means of the fast charge-shifting CCD read-out also directly translates to a better classification performance for differentiation between selected rock types, as e.g. required for geological sample identification in terrestrial as well as extra-terrestrial scenarios. In analogy, the optical lock-in CCD concept is also envisaged to have major beneficial impact in quantification studies where concentration information on sample sub-components is required.

Table 2: PLS-DA classification results for cross-validated data using leave-one-out cross-validation. The optimum number of latent variables (LVs) was automatically selected by SOLO software.

	Charge-shifting (4 LVs)		Conventional (6 LVs)	
	Sensitivity / %	Specificity / %	Sensitivity / %	Specificity / %
Basalt	100	100	100	99
Diorite	95	84.5	60	77
Granite	100	96.9	90	97
Granulite	100	99.0	95	97
Pegmatite	100	82.5	95	80
Quartzite	100	100	100	99
Mean ± SD	99 ± 2	94 ± 8	90 ± 15	92 ± 10

Based on the promising results obtained, it is anticipated that the charge-shifting SERDS technique will be advantageous in a multitude of application fields, where the optical properties of the sample under investigation and/or the measurement conditions are dynamically varying during data acquisition. The technique permits the efficient rejection of disturbing factors not related to Raman scattering, and thus more reliable and more representative spectra of the analyte can be acquired with decreased variation between repeat measurements of the specimen. Using rocks as an example, multivariate data analysis demonstrated that intra-species variability is clearly reduced leading to improved inter-species discrimination performance. This capability is expected to be also beneficial for the distinction between two or more states of a complex matrix, e.g. biological tissue, exhibiting only subtle differences between individual conditions. For example, SERDS in combination with conventional CCD read-out has already been evaluated as a promising method for the classification of healthy and cancerous tissue. [19, 20] It is therefore believed that charge-shifting SERDS combined with multivariate data analysis could pave the way for even more detailed tissue discrimination, e.g. potentially enabling early-stage cancer detection.

3.3. Sub-surface analysis of concealed PTFE layer using SERDS-SORS

In a final set of experiments, the transferability of the charge-shifting SERDS technique for sub-surface analysis was assessed using SORS on a sample consisting of a PTFE layer behind a layer of glossy paper with a multi-colored printed artwork on it. To realize dynamically changing measurement conditions, the specimen was moved by hand during spectral acquisition in an irregular pattern. Using the zero spatial offset configuration, representing a conventional Raman measurement, the spectral signature of the PTFE sub-surface layer could not be recovered through the 0.25 mm thick surface paper layer. Here, the SERDS difference spectra display numerous Raman bands originating from the layer of printed paper itself, i.e. a combination of paper and color pigment Raman bands. Even the strongest

PTFE band located at 732 cm^{-1} was masked irretrievably by the strong spectral signatures of the surface layer (data not shown). In contrast, the SORS measurements at 4 mm spatial offset clearly revealed the Raman signature of the concealed PTFE target layer behind the printed paper as indicated in Figure 6. The contribution of the surface layer was almost completely removed by SORS and only the major surface signals at around 1080 cm^{-1} and 1530 cm^{-1} remained evident as small features in the offset spectra.

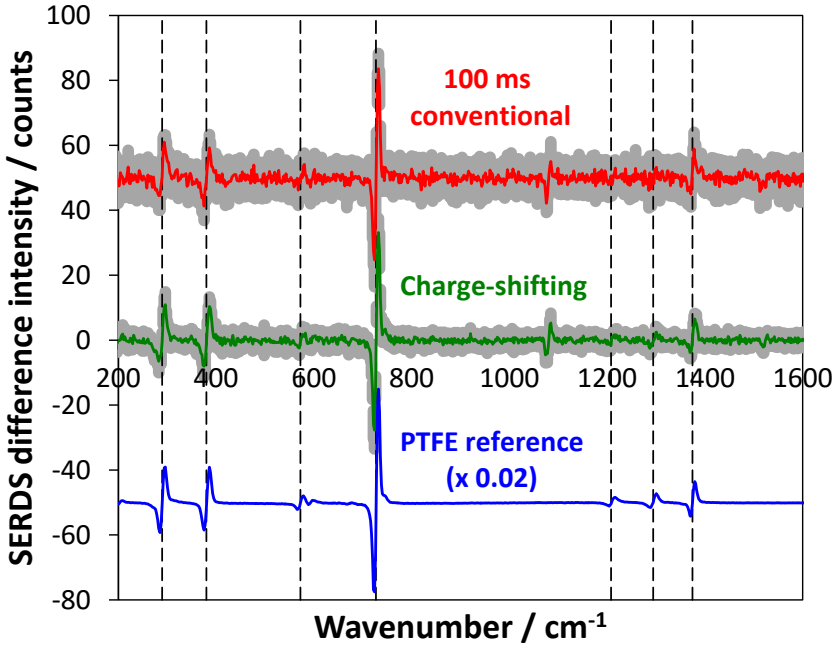

Figure 6: Average SERDS-SORS difference spectra and their standard deviations (grey area) of PTFE block behind printed paper recorded at 4 mm spatial offset for 100 ms conventional read-out and charge-shifting techniques. A scaled reference spectrum of the exposed PTFE using charge-shifting read-out is shown for comparison. The spectra are vertically offset for clarity and vertical dashed lines indicate PTFE Raman bands.

A visual comparison of the averages and standard deviations of 10 SERDS-SORS difference spectra as well as the reconstructed SERDS-SORS spectra recorded in the 4 mm offset configuration highlights that the charge-shifting read-out mode provides a reduced amount of noise (see Figure 6). Due to the low number of total counts in the SORS spectra (and the absence of significant amounts of shot noise as it would be caused by intense fluorescence interference) the read-out noise has a pronounced contribution to the total amount of noise that is present in the spectra with the charge shifting mode yielding a higher S/BG due to its lower overall number of read-out steps. For a quantitative assessment of the spectral quality of the SERDS-SORS difference spectra the signal-to-background-noise-ratio of the major PTFE Raman band at 732 cm^{-1} is plotted against the hit quality index (HQI) [45, 46] in Figure 7. The HQI is a measure to quantify the spectral similarity of the recorded SERDS-SORS spectra of the concealed PTFE block against the SERDS-SORS reference spectrum of the pure PTFE block. The index ranges between 0 and 1 with a score of 1 being a perfect match of test spectrum and reference spectrum. It turns out that the charge-shifting read-out provides clearly superior spectral estimates of the hidden sub-surface layer – even

without the need for a scaled subtraction of the surface spectrum from the sub-surface spectrum, a standard procedure to remove residual surface layer Raman components. Compared to the charge-shifting data the spectra recorded in the conventional read-out mode have an S/BG on average lower by a factor of 2 and they show a 2.2-time lower HQI as well while both read-out modalities have comparable S/N values.

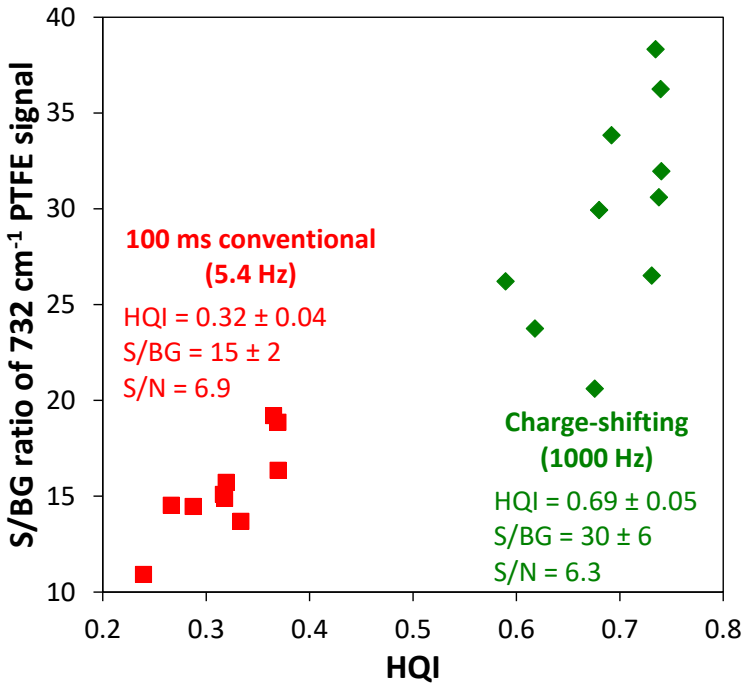

Figure 7: Signal-to-background-noise-ratio of major PTFE Raman band plotted against hit quality index (HQI) for SERDS-SORS difference spectra of PTFE block behind printed paper recorded at 4 mm spatial offset for 100 ms conventional read-out and charge-shifting techniques.

It should be noted that SORS also has an intrinsic capability for fluorescence suppression on condition that the main fluorescence contribution arises from the surface layer. [47] This benefit is however absent where the sub-surface target layer itself is fluorescent. Even if this is not the case for PTFE as selected in this proof-of-concept experiment it is obvious that the charge-shifting SERDS-SORS technique will be most beneficial when surface and sub-surface layers of the sample are fluorescent and heterogeneous.

In our previous study [38] we have demonstrated the ability of the charge-shifting approach to deal with fast varying ambient light interference in Raman spectroscopy. Additionally, SERDS using fast conventional CCD read-out at sub-acquisition times of 200 ms was shown to reject relatively static daylight contributions from Raman spectra. [16, 48] These results together with the very promising outcomes of the present charge-shifting study on heterogeneous specimens highlight the large potential of charge-shifting SERDS (also optionally in combination with SORS) for real-world applications outside the usual laboratory environment where ambient light interference together with fluorescence and sample

heterogeneity are present posing typically major obstacles to effective Raman measurements.

4. Conclusions

This paper highlights the large potential of charge-shifting lock-in CCD read-out applied to SERDS alone and SERDS in combination with SORS for the efficient recovery of Raman spectra, both surface and sub-surface. In a first set of experiments, six different rock types were used as sample material and held in the hand of the operator during measurement to simulate an irregular movement, as e.g. present with hand-held Raman devices. Using the SERDS difference spectra for all 6 heterogeneous rock samples investigated the charge-shifting technique demonstrated superior reproducibility in both univariate and multivariate analysis. As a result, compared to conventional read-out the sensitivity and specificity for the discrimination between the rocks in the charge-shifting mode applying PLS-DA was higher by 9 % and 2 %, respectively – even with a reduced number of latent variables required. This approach would also be expected to be beneficial in Raman applications where quantitative information is required.

A second set of experiments demonstrated the efficient recovery of a spectral signature of PTFE concealed behind a layer of printed paper. Due to the reduced read-out noise in charge-shifting mode, which is particularly relevant for low signal intensities as present in SORS, the signal-to-background-noise-ratio of the sub-surface spectra was higher by a factor of 2 compared to conventional read-out. Applying library-based spectral matching the spectral signature of the hidden PTFE layer could be recovered more than twice as accurate in charge-shifting mode compared to conventional read-out.

Results demonstrated the superior performance of the charge-shifting CCD read-out operated at more than two orders of magnitude higher speeds (1000 Hz) over conventional read-out at 5.4 Hz leading to increased reproducibility between repeat spectra of heterogeneous samples, improved spectral reconstruction and higher signal-to-background-noise-ratio. In combination with ambient light rejection capabilities of the charge-shifting technique, as demonstrated in our previous study, [38] the combination of SERDS and SORS with charge-shifting CCD read-out has a great potential for analysis of heterogeneous specimens outside usual laboratory environments.

Acknowledgement

We wish to thank Dr. André Müller (Ferdinand-Braun-Institut, Leibniz-Institut für Höchstfrequenztechnik) for assistance with the development of the 830 nm microsystem diode laser suitable for SERDS and Andor Technology for provision of the specialized charge-shifting CCD. The support of Dr. Ben Winpenny (The Sedgwick Museum of Earth Sciences (Madingley Rise Site), Cambridge) who provided expert advice in confirming the identity of the investigated rock specimens is greatly appreciated. Finally, we would like to thank Dr.

Sara Mosca (Central Laser Facility, STFC Rutherford Appleton Laboratory) for assistance with the multivariate data analysis.

Conflict of Interest

The authors report there are no conflicts of interest.

Funding

The authors acknowledge the financial support from the UKRI Science and Technology Facilities Council (Proof-of-Concept project PoCF1516-13).

References

1. D. Wei, S. Chen, Q. Liu. "Review of Fluorescence Suppression Techniques in Raman Spectroscopy". Appl. Spectrosc. Rev. 2015. 50(5): 387-406.

2. Y. Chen, L. Dai. "An Automated Baseline Correction Method Based on Iterative Morphological Operations". Appl. Spectrosc. 2018. 72(5): 731-739.

3. S. Giguere , T. Boucher , C.J. Carey , S. Mahadevan, M.D. Dyar. "A Fully Customized Baseline Removal Framework for Spectroscopic Applications". Appl. Spectrosc. 2017. 71(7): 1457-1470.

4. E.V. Efremov, J.B. Buijs, C. Gooijer, F. Ariese. "Fluorescence Rejection in Resonance Raman Spectroscopy Using a Picosecond-Gated Intensified Charge-Coupled Device Camera". Appl. Spectrosc. 2007. 61(6): 571-578.

5. C.J. Corden, D.W. Shipp, P. Matousek, I. Notingher. "Fast Raman Spectral Mapping of Highly Fluorescing Samples by Time-Gated Spectral Multiplexed Detection". Opt. Lett. 2018. 43(23): 5733-5736.

6. P. Matousek, M. Towrie, A. Stanley, A.W. Parker. "Efficient Rejection of Fluorescence from Raman Spectra Using Picosecond Kerr Gating". Appl. Spectrosc. 1999. 53(12): 1485-1489.

7. P. Matousek, M. Towrie, A.W. Parker. "Simple Reconstruction Algorithm for Shifted Excitation Raman Difference Spectroscopy". Appl. Spectrosc. 2005. 59(6): 848-851.

8. A.P. Shreve, N.J. Cherepy, R.A. Mathies. "Effective Rejection of Fluorescence Interference in Raman Spectroscopy Using a Shifted Excitation Difference Technique". Appl. Spectrosc. 1992. 46(4): 707-711.

9. J. Zhao, M.M. Carrabba, F.S. Allen. "Automated Fluorescence Rejection Using Shifted Excitation Raman Difference Spectroscopy". Appl. Spectrosc. 2002. 56(7): 834-845.

10. J.B. Cooper, M. Abdelkader, K.L. Wise. "Sequentially Shifted Excitation Raman Spectroscopy: Novel Algorithm and Instrumentation for Fluorescence-Free Raman Spectroscopy in Spectral Space". Appl. Spectrosc. 2013. 67(8): 973-984.

11. S.T. McCain, R.M. Willett, D.J. Brady. "Multi-Excitation Raman Spectroscopy Technique for Fluorescence Rejection". Opt. Express. 2008. 16(15): 10975-10991.

12. M. Maiwald, B. Sumpf. "Shifted Excitation Raman Difference Spectroscopy - From Diode Lasers to In-Situ Applications". Proc. SPIE. 2018. 10509: 1050903-1-1050903-11.

13. C. Conti, A. Botteon, M. Bertasa, C. Colombo, M. Realini, D. Sali. "Portable Sequentially Shifted Excitation Raman Spectroscopy as an Innovative Tool for In Situ Chemical Interrogation of Painted Surfaces". Analyst. 2016. 141(15): 4599-4607.

14. A. Culka, J. Jehlička. "Sequentially Shifted Excitation: A Tool for Suppression of Laser-Induced Fluorescence in Mineralogical Applications Using Portable Raman Spectrometers". J. Raman Spectrosc. 2018. 49(3): 526-537.

15. K. Sowoidnich, H.-D. Kronfeldt. "Shifted Excitation Raman Difference Spectroscopy at Multiple Wavelengths for In-Situ Meat Species Differentiation". Appl. Phys. B. 2012. 108(4): 975-982.

16. M. Maiwald, A. Müller, B. Sumpf, G. Tränkle. "A Portable Shifted Excitation Raman Difference Spectroscopy System: Device and Field Demonstration". J. Raman Spectrosc. 2016. 47(10): 1180-1184.

17. B. Volodin, S. Dolgy, V.S. Ban, D. Gracin, K. Juraic, L. Gracin. "Application of the Shifted Excitation Raman Difference Spectroscopy (SERDS) to the Analysis of Trace Amounts of Methanol in Red Wines". Proc. SPIE. 2014. 8939: 89390Y-1-89390Y-10.

18. M. Maiwald, B. Sumpf, G. Tränkle. "Rapid and Adjustable Shifted Excitation Raman Difference Spectroscopy Using a Dual-Wavelength Diode Laser at 785 nm". J. Raman Spectrosc. 2018. 49(11): 1765-1775.

19. C. Knipfer, J. Motz, W. Adler, K. Brunner, M.T. Gebrekidan, R. Hankel, A. Agaimy, S. Will, A. Braeuer, F.W. Neukam, F. Stelzle. "Raman Difference Spectroscopy: A Non-Invasive Method for Identification of Oral Squamous Cell Carcinoma". Biomed. Opt. Express. 2014. 5(9): 3252-3265.

20. E. Schmälzlin, B. Moralejo, D. Bodenmüller, M.E. Darvin, G. Thiede, M.M. Roth. "Ultrafast Imaging Raman Spectroscopy of Large-Area Samples Without Stepwise Scanning". J. Sens. Sens. Syst. 2016. 5(2): 261-271.

21. M.T. Gebrekidan, C. Knipfer, F. Stelzle, J. Popp, S. Will, A. Braeuer. "A Shifted-Excitation Raman Difference Spectroscopy (SERDS) Evaluation Strategy for the Efficient Isolation of Raman Spectra from Extreme Fluorescence Interference". J. Raman Spectrosc. 2016. 47(2): 198-209.

22. E. Cordero, F. Korinth, C. Stiebing, C. Krafft, I.W. Schie, J. Popp. "Evaluation of Shifted Excitation Raman Difference Spectroscopy and Comparison to Computational Background Correction Methods Applied to Biochemical Raman Spectra". Sensors. 2017. 17(8): 1724.

23. M. Braune, M. Maiwald, M.E. Darvin, B. Eppich, B. Sumpf, J. Lademann, G. Tränkle. "Shifted Excitation Resonance Raman Difference Spectroscopy System Suitable for the Quantitative In Vivo Detection of Carotenoids in Human Skin". Laser Phys. Lett. 2018. 15(11): 115601.

24. M. Maiwald, H. Schmidt, B. Sumpf, R. Güther, G. Erbert, H.-D. Kronfeldt, G. Tränkle. "Microsystem Light Source at 488 nm for Shifted Excitation Resonance Raman Difference Spectroscopy". Appl. Spectrosc. 2009. 63(11): 1283-1287.

25. C.A. Tracewell, A. Cua, D.H. Stewart, D.F. Bocian, G.W. Brudvig. "Characterization of Carotenoid and Chlorophyll Photooxidation in Photosystem II". Biochemistry. 2001. 40(1): 193-203.

26. H. Ahmad, H.-D. Kronfeldt. "High Sensitive Seawater Resistant SERS Substrates Based on Gold Island Film Produced by Electroless Plating". Marine Science. 2013. 3(1): 1-8.

27. Y.-H. Kwon, K. Sowoidnich, Z. Wu, H.-D. Kronfeldt. "Innovative SERS/SERDS Concept for Chemical Trace Detection in Sea-Water". Int. J. Offshore Polar. 2017. 27(3): 225-231.

28. J. Register, M. Maiwald, A. Fales, P. Strobbia, B. Sumpf, T. Vo-Dinh. "Shifted-Excitation Raman Difference Spectroscopy for the Detection of SERS-Encoded Gold Nanostar Probes". J. Raman Spectrosc. 2018. 49(12): 1961-1967.

29. U. Böttger, M. Maiwald, F. Hanke, M. Braune, S.G. Pavlova, S. Schröder, I. Weber, H. Busemann, B. Sumpf, G. Tränkle, H.-W. Hübers. "Shifted Excitation Raman Difference Spectroscopy Applied to Extraterrestrial Particles Returned from the Asteroid Itokawa". Planet. Space Sci. 2017. 144: 106-111.

30. K. Noack, B. Eskofier, J. Kiefer, C. Dilk, G. Bilow, M. Schirmer, R. Buchholz, A. Leipertz. "Combined Shifted-Excitation Raman Difference Spectroscopy and Support Vector Regression for Monitoring the Algal Production of Complex Polysaccharides". Analyst. 2013. 138(19): 5639-5646.

31. I. Osticioli, A. Zoppi, E.M. Castellucci. "Shift-Excitation Raman Difference Spectroscopy-Difference Deconvolution Method for the Luminescence Background Rejection from Raman Spectra of Solid Samples". Appl. Spectrosc. 2007. 61(8): 839-844.

32. M. Maiwald, J. Fricke, A. Ginolas, J. Pohl, B. Sumpf, G. Erbert, G. Tränkle. "Monolithic Y-Branch Dual-Wavelength DBR Diode Laser at 671 nm for Shifted Excitation Raman Difference Spectroscopy". Proc. SPIE. 2013. 8718: 871808-1-871808-11.

33. M. Maiwald, H. Schmidt, B. Sumpf, G. Erbert, H.-D. Kronfeldt, G. Tränkle. "Microsystem 671 nm Light Source for Shifted Excitation Raman Difference Spectroscopy". Appl. Opt. 2009. 48(15): 2789-2792.

34. M. Maiwald, B. Eppich, A. Ginolas, B. Sumpf, G. Erbert, G. Tränkle. "Compact Handheld Probe for Shifted Excitation Raman Difference Spectroscopy with Implemented Dual-Wavelength Diode Laser at 785 Nanometers". Appl. Spectrosc. 2015. 69(10): 1144-1151.

35. H.P. Povel, H. Aebersold, J.O. Stenflo. "Charge-Coupled Device Image Sensor as a Demodulator in a 2-D Polarimeter with a Piezoelastic Modulator". Appl. Opt. 1990. 29(8): 1186-1190.

36. H.P. Povel, C.U. Keller, I.-A. Yadigaroglu. "Two-Dimensional Polarimeter with a Charge-Coupled-Device Image Sensor and a Piezoelastic Modulator". Appl. Opt. 1994. 33(19): 4254-4260.

37. R. Heming, H. Herzog, V. Deckert. "Optical CCD Lock-In Device for Raman Difference Spectroscopy". DGaO Proceedings. 2008. 109: P33.

38. K. Sowoidnich, M. Towrie, P. Matousek. "Charge-Shifting CCD Read-Out Concept for the Rejection of Varying Ambient Light Interference from Raman Spectra". J. Raman Spectrosc. 2019. DOI: 10.1002/jrs.5597.

39. P. Matousek, I.P. Clark, E.R.C. Draper, M.D. Morris, A.E. Goodship, N. Everall, M. Towrie, W.F. Finney, A.W. Parker. "Subsurface Probing in Diffusely Scattering Media Using Spatially Offset Raman Spectroscopy". Appl. Spectrosc. 2005. 59(4): 393-400.

40. M. Chen, J. Mas, L.H. Forbes, M.R. Andrews, K. Dholakia. "Depth-Resolved Multimodal Imaging: Wavelength Modulated Spatially Offset Raman Spectroscopy with Optical Coherence Tomography". J. Biophotonics. 2018. 11(1): e201700129.

41. B. Sumpf, A. Müller, M. Maiwald. "Tailored Diode Lasers - Enabling Raman Spectroscopy in the Presence of Disturbing Fluorescence and Background Light". Proc. SPIE. 2019. 10894: 1089411-1-1089411-8.

42. A. Wang, B. L. Jolliff, L. A. Haskin. "Raman Spectroscopic Characterization of a Highly Weathered Basalt: Igneous Mineralogy, Alteration Products, and a Microorganism". J. Geophys. Res. 1999. 104(E11): 27067-27077.

43. M. Enami, T. Nishiyama, T. Mouri. "Laser Raman Microspectrometry of Metamorphic Quartz: A Simple Method for Comparison of Metamorphic Pressures". Am. Mineral. 2007. 92(8-9): 1303-1315.

44. J. Mihály, S. Sterkel, H. M. Ortner, L. Kocsis, L. Hajba, É. Furdyga, J. Mink. "FTIR and FT-Raman Spectroscopic Study on Polymer Based High Pressure Digestion Vessels". Croat. Chem. Acta. 2006. 79(3): 497-501.

45. J.D. Rodriguez, B.J. Westenberger, L.F. Buhse, J.F. Kauffman. "Standardization of Raman Spectra for Transfer of Spectral Libraries Across Different Instruments". Analyst. 2011. 136(20): 4232-4240.

46. S. Lee, H. Lee, H. Chung. "New Discrimination Method Combining Hit Quality Index Based Spectral Matching and Voting". Anal. Chim. Acta. 2013. 758: 58-65.

47. C. Conti, A. Botteon, C. Colombo, M. Realini, P. Matousek. "Fluorescence Suppression Using Micro-Scale Spatially Offset Raman Spectroscopy". Analyst. 2016. 141(18): 5374-5381.

48. M. Maiwald, A. Müller, B. Sumpf, G. Erbert, G. Tränkle. "Capability of Shifted Excitation Raman Difference Spectroscopy Under Ambient Daylight". Appl. Opt. 2015. 54(17): 5520-5524.